Earth's Future

RESEARCH ARTICLE
10.1029/2023EF003982

Fast Transit of Carbon Inputs in Global Soil Profiles Regardless of Entering Depth

Guocheng Wang[1,2,3], Mingming Wang[4], Liujun Xiao[4], Carlos A. Sierra[5,6], Jinfeng Chang[4,7,8], Zhou Shi[4,7,8], and Zhongkui Luo[4,7,8]

[1]Faculty of Geographical Science, Beijing Normal University, Beijing, China, [2]State Key Laboratory of Earth Surface Processes and Resource Ecology, Beijing Normal University, Beijing, China, [3]Center for Geodata and Analysis, Beijing Normal University, Beijing, China, [4]Institute of Agricultural Remote Sensing and Information Technology, College of Environment and Resource Sciences, Zhejiang University, Hangzhou, China, [5]Max Planck Institute for Biogeochemistry, Jena, Germany, [6]Department of Ecology, Swedish University of Agricultural Sciences, Uppsala, Sweden, [7]Academy of Ecological Civilization, Zhejiang University, Hangzhou, China, [8]Key Laboratory of Environment Remediation and Ecological Health, Ministry of Education, Zhejiang University, Hangzhou, China

Abstract Climate and land management changes are altering carbon inputs to soil. The consequence of such input changes on long-term soil organic carbon (SOC) balance depends on the transit behavior of carbon inputs. Using observational carbon input and radiocarbon data in global soil profiles, we reveal that on average nearly 25% of new entering carbon leave soil in 1 year irrespective of entering depth, and the remained fraction after 30 years is only ~13%. Nevertheless, the majority of SOC is older than 30 years in all soil depths. Together, these results demonstrate low transfer efficiency of carbon inputs to aged SOC which is the meaningful carbon component for long-term SOC sequestration. Additionally, we reveal that SOC aging and carbon input transiting are two distinct processes, which should be simultaneously, but mechanistical-separately, considered to predict and manage SOC dynamics in response to carbon input changes under climate and land management changes.

Plain Language Summary Soil contains a lot of carbon, and its levels can change based on climate and how we manage the land. Our global soil research shows that when new carbon goes into the soil, about 25% of it leaves within a year, regardless of depth. After 30 years, only about 13% remains. Interestingly, most of the carbon in the soil is older than 30 years, showing that it can store carbon for a long time. We found that transferring carbon inputs to aged soil organic carbon (SOC) is not very efficient. This aged SOC is crucial for long-term carbon storage, which can help combat climate change. We also discovered that SOC aging and carbon input transit are separate processes. To manage soil carbon well in response to climate and land changes, we need to consider these processes separately but at the same time. In conclusion, our research reveals how carbon behaves in soil and stresses the importance of aged SOC for long-term carbon storage. Understanding these processes better can lead to more effective strategies for managing and protecting our soils, contributing to the fight against climate change.

Key Points:

- Around 80% of carbon inputs leave soil in 10 years after entering and do not contribute to aged soil carbon component
- The low transfer efficiency of carbon inputs to aged soil carbon undermines the feasibility of managing carbon inputs for soil carbon sequestration
- The dynamics of new carbon inputs and aged soil carbon are influenced by distinct climatic and edaphic attributes

Supporting Information:

Supporting Information may be found in the online version of this article.

Correspondence to:

Z. Luo,
luozk@zju.edu.cn

Citation:

Wang, G., Wang, M., Xiao, L., Sierra, C. A., Chang, J., Shi, Z., & Luo, Z. (2024). Fast transit of carbon inputs in global soil profiles regardless of entering depth. *Earth's Future*, *12*, e2023EF003982. https://doi.org/10.1029/2023EF003982

Received 17 JULY 2023
Accepted 30 JAN 2024

Author Contributions:

Conceptualization: Zhongkui Luo
Data curation: Guocheng Wang, Liujun Xiao, Zhongkui Luo
Formal analysis: Guocheng Wang
Funding acquisition: Jinfeng Chang, Zhou Shi, Zhongkui Luo
Investigation: Guocheng Wang
Methodology: Mingming Wang, Carlos A. Sierra, Zhongkui Luo
Project administration: Zhongkui Luo
Resources: Liujun Xiao, Zhongkui Luo
Writing – original draft: Guocheng Wang, Zhongkui Luo

1. Introduction

The balance between carbon inputs from plant photosynthesis and carbon outputs mainly from soil microbial respiration determines the dynamics of soil organic carbon (SOC). Climate and land use/management changes can affect both carbon inputs and outputs (Song et al., 2019; Terrer et al., 2021). This may lead to soil carbon accumulation or loss, which has significant implications for climate through regulating atmospheric CO_2 levels and for global production of food, feed and fiber through influencing soil fertility (Lal, 2004). However, it is challenging to experimentally monitor carbon inputs and outputs down the soil profile and across large spatial scales (Jobbágy & Jackson, 2000), as they are transient, subtle, and strongly influenced by environmental conditions (Crowther et al., 2016; Jackson et al., 2017; Terrer et al., 2019). Moreover, soil carbon consists of various organic compounds with different ages (i.e., the time a carbon atom has spent in soil since entering it) (Lehmann & Kleber, 2015). Without detailed information about how carbon inputs transit to different age groups of SOC, we cannot reliably predict the persistence of carbon inputs and develop management practices for effective long-term carbon sequestration and sustainable ecosystem services provisioned by soils.

When carbon atoms enter soil in plant-derived organic materials, some of them may leave soil in a short time due to physical transport or preferential microbial utilization (i.e., fast transit time), and some may stay for a longer

Writing – review & editing:
Mingming Wang, Liujun Xiao, Carlos A. Sierra, Jinfeng Chang, Zhou Shi

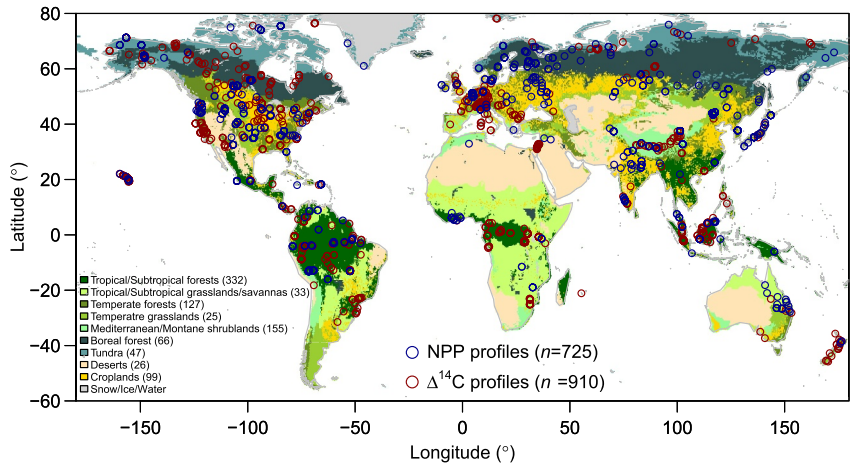

Figure 1. Location of measurements of net primary productivity (NPP) and soil radiocarbon content ($\Delta^{14}C$). Values in parentheses show the number of profiles for each of the two data sets. Sample size of radiocarbon measurements for each biome is shown in the parentheses following the biome legend.

period due to microbial recycling, stabilization or protection offered by soil matrixes (i.e., slow transit time) (Sierra et al., 2017). The transit time of new carbon atoms entering soil varies in space and time, and determines how much and to what extent carbon input contributes to old carbon and thus to long-term SOC stabilization. If most carbon inputs transit fast, for example, changes in SOC stock induced by carbon input would be negligible in the short term, and only detectable at long time scales when significant amounts have accumulated for enough time (usually centuries or millennia in most soils (Luo et al., 2019)). However, it is difficult to quantify the subtle transit process of carbon inputs. The main challenge is that carbon fluxes derived from the decomposition of carbon inputs are mixed with autotrophic respiration of plant roots and heterotrophic respiration of microbial decomposition derived from native SOC. For the transit of carbon inputs in different soil depths, we face a more difficult challenge of separating carbon fluxes from different soil depths. Carbon isotope observations can be used to estimate mean ages of SOC (Balesdent et al., 2018; Shi et al., 2020) or trace short-term dynamics of labeled carbon substrates entering soil. Nevertheless, carbon isotope measurements alone do not allow tracking the continuous long-term transit of carbon inputs.

We used a data-model integration approach to estimate quantitatively how carbon inputs transit and contribute to different age groups of SOC across soil depths. This estimation builds on previous approaches for inferring mean ages of SOC ($\bar{a}$) and mean transit time of carbon inputs ($\bar{\tau}$, which describes the age of a carbon atom at the time it leaves soil) in each soil depth for each soil profile (Carvalhais et al., 2014; Luo et al., 2019; Shi et al., 2020; Xiao et al., 2022). We first estimated $\bar{a}$ and $\bar{\tau}$ using global radiocarbon measurements in 910 soil profiles from the International Soil Radiocarbon Databased (ISRaD) (Lawrence et al., 2020) (Figure 1) and observational carbon inputs (Xiao et al., 2023). Then we derived decay rates and transfer coefficients for a two-pool carbon model—Inventory Carbon Balance Model (ICBM) (Andrén & Kätterer, 1997) using the estimated $\bar{a}$ and $\bar{\tau}$. Finally, the distribution of transit times (τ) of carbon inputs and the age structure of SOC (a) are constructed using the derived decay rates and transfer coefficients (Metzler & Sierra, 2018).

2. Materials and Methods

We used a two-step approach for obtaining ages and transit times. In a first step, we obtained empirical estimates of mean age and mean transit time using the set of observations as described in Sections 2.2 and 2.3. These estimates of mean age and mean transit time are based on the assumption of a one-pool model. Because these obtained estimates differ considerably among each other despite the fact that for a one-pool model both should be equal, then we proceeded to fit parameters of a two-pool model to the empirical estimates of mean age and mean transit time. The two pool model reconciles these differences and allowed us to obtain complete age and transit time distributions. In the following, we describe the main equations and theory, and how the data was used in the data-assimilation procedure.

2.1. Distributions of Soil Carbon Age (a) and Carbon Input Transit Time (τ)

Carbon models are needed to characterize the distribution of a and τ. Amongst them, pool-based models are widely used. In general, these models can be expressed in matrix form as:

$$\frac{d\mathbf{C}}{dt} = \mathbf{I} + \mathbf{A} \cdot \mathbf{C}, \tag{1}$$

where $\mathbf{C}$ and $\mathbf{I}$ are vectors of carbon pools and corresponding carbon inputs to them, respectively; $\mathbf{A}$ is a matrix defining the cycling and transfer among the pools. At steady state, Metzler and Sierra (2018) have proved that the probability density function (PDF) of soil carbon age (a, which is defined as the time a carbon atom has experienced since the carbon atom entered soil) can be computed as:

$$f(a) = -(1,\ldots,1)^{\mathrm{T}} \cdot \mathbf{A} \cdot e^{a \cdot \mathbf{A}} \cdot \frac{\mathbf{C}^*}{\sum \mathbf{C}^*}, a \geq 0, \tag{2}$$

and mean soil carbon age ($\overline{a}$) can be calculated as:

$$\overline{a} = -(1,\ldots,1)^{\mathrm{T}} \cdot \mathbf{A}^{-1} \cdot \frac{\mathbf{C}^*}{\sum \mathbf{C}^*}, \tag{3}$$

where $(1, \ldots, 1)^{\mathrm{T}}$ is the transpose of a vector containing ones with the vector length being equal to the number of carbon pools; $\mathbf{C}^* = -\mathbf{A}^{-1} \cdot \mathbf{I}$ represent the steady-state solution of the model (i.e., the sizes of carbon pools at steady state). The PDF of carbon input transit time (τ, which is defined as the time elapsed since carbon atom entered soil until it exists via any efflux pathways) can be calculated as:

$$f(\tau) = -(1,\ldots,1)^{\mathrm{T}} \cdot \mathbf{A} \cdot e^{\tau \cdot \mathbf{A}} \cdot \frac{\mathbf{I}}{\sum \mathbf{I}}, \tau \geq 0, \tag{4}$$

and mean soil carbon transit time ($\overline{\tau}$) can be calculated as:

$$\overline{\tau} = -(1,\ldots,1)^{\mathrm{T}} \cdot \mathbf{A}^{-1} \cdot \frac{\mathbf{I}}{\sum \mathbf{I}}. \tag{5}$$

In this study, a widely used two-pool carbon model ICBM (Andrén & Kätterer, 1997) which divides total soil carbon into a fast (C_f) and slow (C_s) pool was used. Explicitly, the matrix and vector form of the model can be written as:

$$\begin{pmatrix} \frac{dC_f}{dt} \\ \frac{dC_s}{dt} \end{pmatrix} = \begin{pmatrix} I_f \\ 0 \end{pmatrix} + \begin{pmatrix} -k_f & 0 \\ \alpha \cdot k_f & -k_s \end{pmatrix} \cdot \begin{pmatrix} C_f \\ C_s \end{pmatrix}, \tag{6}$$

where I_f is the amount of carbon input allocated to C_f; k_f and k_s are the decay rates of the two pools, respectively; α is the transfer coefficient. At steady state, according to Equations 3 and 5, mean soil carbon age ($\overline{a}$) and transit time ($\overline{\tau}$) estimated by this model can be computed, respectively, as:

$$\overline{a} = \frac{1}{k_f} + \frac{1}{k_s} - \frac{1}{k_f \cdot \alpha + k_s}, \tag{7}$$

and

$$\overline{\tau} = \frac{1}{k_f} + \frac{\alpha}{k_s}, \tag{8}$$

Based on Equations 7 and 8, if $\overline{a}$ and $\overline{\tau}$ can be determined, we can constrain k_f, k_s and α thereby the PDF of a and τ using Equations 2 and 4, respectively. However, the two equations (i.e., Equations 7 and 8) do not allow us to obtain a unique solution for the three parameters. Rather, numerous parameter ensembles exist to match $\overline{a}$ and $\overline{\tau}$ (i.e., parameter equifinality). We explicitly quantify the effects of such equifinality on the estimation of PDF of a and τ (see Section 2.4).

2.2. Estimation of Mean Soil Carbon Age ($\overline{a}$)

We used a radiocarbon modeling approach to estimate $\overline{a}$ using the updated ISRaD database (Lawrence et al., 2020). In the new version of the database, there are a total of 910 soil profiles with 5,160 Δ^{14}C measurements of SOC in different soil layer depths. A one-pool radiocarbon model can be used to estimate $\overline{a}$ as the inverse of the fitted decay rate (i.e., 1/k) of SOC (Cherkinsky & Brovkin, 1993; Xiao et al., 2022):

$$F_{\mathrm{soil},t} \cdot C_t = F_{I,t} \cdot I_t - F_{\mathrm{soil},t-1} \cdot C_{t-1} \cdot (1 - k - \gamma), \tag{9}$$

where $F_{\mathrm{soil},t}$ and $F_{I,t}$ are the $^{14}C/^{12}C$ ratio of the modern reference (i.e., fraction modern) in SOC and carbon input to soil at time t, respectively; C_t and I_t are the amounts of SOC stock and carbon input to soil at time t, respectively; k is the decay rate of SOC; and γ is the β-decay rate of ^{14}C and equals to 1/8,267 per year. At steady state, both I_t and C_t are constant. That is, $C_t = C_{t-1} = I_t/k$, and Equation 9 can be reduced to:

$$F_{\mathrm{soil},t} = F_{I,t} \cdot k - F_{\mathrm{soil},t-1} \cdot (1 - k - \gamma). \tag{10}$$

Using the Δ^{14}C data, which is reported as the per mille deviation from a standard of fixed isotopic composition, F for either SOC or carbon input can be calculated as:

$$F = \frac{\Delta^{14}\mathrm{C}}{1{,}000} + 1. \tag{11}$$

The one-pool model treats SOC in each layer as a homogeneous cohort and was fitted to observed Δ^{14}C values. A steady state of radiocarbon at the beginning of the modeling (i.e., 50,000 BP) was assumed and the model was ran at half-year time step to the year of soil Δ^{14}C measurement using atmospheric Δ^{14}C as inputs, and k was iteratively solved to match observed F values of SOC. Historical northern and southern hemisphere atmospheric Δ^{14}C records (50,000 to 0 BP) were obtained from IntCal20 (Reimer et al., 2020) and SHCal20 (Hogg et al., 2020), respectively. Modern atmospheric Δ^{14}C from 1950 to 2019 for both northern and southern hemisphere were obtained from Hua et al. (2021). Depending on the measurement year of SOC, the model generated two $\overline{a}$ values for some positive large Δ^{14}C values (i.e., fast turnover of SOC) due to the ascending and then descending of Δ^{14}C during and after the bomb-test. The longer one was used in the estimation. $\overline{a}$ was estimated for recorded depth intervals in the ISRaD database. To provide more details about the depth distribution of $\overline{a}$, we also calculated $\overline{a}$ for each 10 cm depth interval in the 0–200 cm profile. To do so, Δ^{14}C was interpolated to the 10 cm depth intervals using mass-preserving splines (Bishop et al., 1999). Depending on the depth of observed profiles, depth was truncated to the deepest depth which the recorded depth interval can cover. To further ease comparison among soil profiles and with other studies, based on the depth distribution of $\overline{a}$, we also calculated $\overline{a}$ for three common soil depth intervals (i.e., 0–30 cm, 30–100 cm and 100–200 cm) which are widely used in the literature (Balesdent et al., 2018; Luo et al., 2019; Shi et al., 2020). For $\overline{\tau}$ (see Section 2.3), it has been also calculated for these depth intervals using the same depth interpolation approach.

2.3. Estimation of Mean Transit Time of Carbon Input ($\overline{\tau}$)

Assuming steady state, mean transit time of carbon inputs ($\overline{\tau}$) in any layer depths can be calculated as the ratio of soil carbon stock to carbon input to that layer (Sierra et al., 2017, 2018):

$$\tau_i = \frac{\mathrm{SOC}_{s,i}}{\mathrm{Input}_i}, \tag{12}$$

where $\mathrm{SOC}_{s,i}$ is the SOC stock in the ith soil layer, and Input_i is the amount of carbon input to that layer.

We estimated $\bar{\tau}$ for each recorded depth interval at the locations of the $\Delta^{14}C$ profiles corresponding to the 5,160 $\Delta^{14}C$ measurements. The recorded SOC stock, if available and can be estimated, was used for SOC_s. For 541 out of the 5,160 $\Delta^{14}C$ measurements, SOC_s is not reported or cannot be estimated using reported data, we used the WISE30sec database (Batjes, 2016), which is a mapping product of global SOC stocks in different soil depths at 0.0083° (i.e., ∼1 km at the equator) resolution, to fill this data gap.

We estimated carbon inputs (Input) to each soil layer using a machine learning model validated by Xiao et al. (2023). This model assumes that Input is mainly determined by the depth allocation of belowground net primary production (BNPP), which follows the depth distribution of root biomass and turnover. It also accounts for vertical carbon transport (V) along the soil profile due to leaching and/or bioturbation, using a partial differential equation (Koven et al., 2013; Xiao et al., 2022). In the top layer, we added 10% of aboveground NPP (ANPP) to Input (i.e., Input = BNPP + V + 0.1 × ANPP) (Xiao et al., 2022). We developed a predictive model for BNPP depth allocation using in situ measurements at 725 global locations (Figure 1). We applied this model to predict Input at the locations of $\Delta^{14}C$ measurements. A detailed description of the BNPP data sets and the modeling for the depth allocation of BNPP can be found in Xiao et al. (2023).

2.4. Estimation of the PDF of a and τ

Using the estimated $\bar{a}$ and $\bar{\tau}$, we fitted Equations 7 and 8 to derive three parameters: k_f—the decay rate of fast pool, k_s—the decay rate of slow pool, and α—the transfer coefficient of fast pool to the slow pool. For both k_f and k_s, a prior range of from 0 (which is equivalent to a turnover time of ∞) to 1 (which is equivalent to a turnover time of 1 year) was assigned. For α, it ranges from 0.2 to 0.8. From these priors, a total of 1,000 ensembles of the three parameters were obtained by optimizing the two equations using a differential evolution optimization approach (Vrugt & Ter Braak, 2011). These ensembles represent uncertainties in the three parameters due to insufficient data to get unique solutions for them. This uncertainty was brought into the calculation of the PDF of a and τ using Equations 2 and 4. Specifically, for each soil depth interval in each soil profile, we calculated PDF of soil carbon age and carbon input transit time. Then, the PDF was used to calculate the probability density of a (i.e., a < 1 year, 1 year < a < 10 years, 10 years < a < 30 years, 30 years < a < 100 years, 100 years < a < 200 years, 200 years < a < 500 years, 500 years < a < 1,000 years, and a > 1,000 years) and τ of interests (i.e., τ < 1 year, τ > 1 year, 1 year < τ < 10 years, 10 years < τ < 30 years, τ > 30 years, 30 years < τ < 100 years, 100 years < τ < 200 years, 200 years < τ < 500 years, 500 years < τ < 1,000 years, and τ > 1,000 years). These probability densities represent the integrals (areas under the PDF curve) for specific intervals of a and τ, respectively. We also calculated the ratio of $a_{>1{,}000\ \text{years}}$:$a_{<10\ \text{years}}$ and $\tau_{>30\ \text{years}}$:$\tau_{>1\ \text{year}}$ to indicate the age structure of soil carbon and transit behavior of carbon inputs.

2.5. Controls on Age Structures of Soil Carbon and Transit Times of Carbon Inputs

To identify the potential factors influencing soil carbon age and transit times, we selected a range of climatic, edaphic and topographic variables (Table S1 in Supporting Information S1). We obtained 20 soil properties from ISRIC-WISE (International Soil Reference and Information Centre-World Inventory of Soil Emission Potentials) soil profile database (Batjes, 2016) and 19 climatic attributes (including mean annual temperature and precipitation) from WorldClim database (Fick & Hijmans, 2017), both at a spatial resolution of ∼1 km. We also used 13 topographic attributes from Amatulli et al. (2018). Moreover, we derived biome type following Luo et al. (2019) and extracted soil order data from Global Soil Regions Map database. We matched these environmental covariates with the $\Delta^{14}C$ data from ISRaD database at their locations.

In the present study, we calculated $a_{>1{,}000\ \text{years}}$:$a_{<10\ \text{years}}$ to illustrate the age structure of soil carbon, focusing on the comparison between older groups (aged over 1,000 years) and younger groups (under 10 years). Regarding τ, we determined $\tau_{>30\ \text{years}}$:$\tau_{>1\ \text{year}}$ to reveal its structure by quantifying the groups of soil carbon inputs that are notably significant for soil carbon sequestration (e.g., longer than 30 years) within the categories with considerably long transit times (e.g., longer than 1 year). Focusing on $\tau_{>30\ \text{years}}$:$\tau_{>1\ \text{year}}$ and $a_{>1{,}000\ \text{years}}$:$a_{<10\ \text{years}}$ in the 0–30, 30–100, and 100–200 cm soil depths, variation partitioning analysis (VPA) was used to explore the relative importance of climate, soil and topography in influencing these two ratios. VPA identifies the individual contributions of independent variables to a dependent variable (Peres-Neto et al., 2006). We controlled multicollinearity of the environmental covariates by calculating variance inflation factor (VIF) (Zuur et al., 2010) and removing the variable with the highest VIF until all VIFs were less than 10. We selected environmental variables

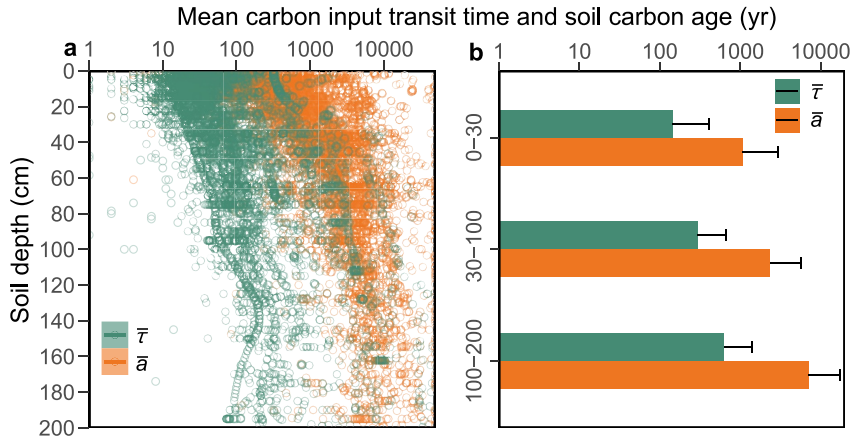

Figure 2. Depth distribution of mean transit times of carbon input ($\overline{\tau}$) and mean soil carbon ages ($\overline{a}$). (a) At each location of $\Delta^{14}C$ measurements, the middle depth of sampling depth interval (i.e., top and bottom depths) was used to represent soil depth. (b) $\Delta^{14}C$ observations were harmonized to three standard soil layer depths (0–30, 30–100, and 100–200 cm), and then the harmonized $\Delta^{14}C$ values were used to predict $\overline{a}$ using a one-pool soil radiocarbon model. $\overline{\tau}$ was calculated using soil carbon stock divided by carbon input in each soil layer at each location (Methods). Error bars in (b) show one standard deviation.

that best explain the dependent variable (i.e., the two ratios) using redundancy analyses and analyses of variance. We used a stepwise permutational ordination method (the *ordistep* function in *vegan* package) with 1,000 permutations to evaluate the environmental variables and create a model. We performed VPA using these selected environmental variables and the *varpart* function in the R package *vegan*. We conducted all these statistical assessments in R 4.2.5 (R Development Core Team, 2023).

2.6. Sensitivity Analyses and Uncertainty Assessment

We performed three additional analyses to evaluate the sensitivity of the estimated PDF of τ and a to aspects of the analytical method. First, we tested how the PDF of τ and a responds to the uncertainty in $\overline{a}$ estimates. In this study, we used a one-pool radiocarbon model to infer $\overline{a}$ using the $\Delta^{14}C$ measurement for each soil depth in each soil profile. Using two-pool mixing radiocarbon models, previous authors have demonstrated $\overline{a}$ will become uncertain and $\overline{a}$ estimated by the one-pool model is within the lower range of the mean ages estimated by the two-pool model (Shi et al., 2020). To explore the potential uncertainty induced by such discrepancy, the estimation of the PDF was repeated using $\overline{a} \pm 10\%$. Similarly, we also test how the PDFs of τ and a respond to uncertainties in $\overline{\tau}$ by repeating $\overline{\tau} \pm 10\%$. Second, we included an independent MODIS (Moderate Resolution Imaging Spectroradiometer) NPP-based carbon input data set (Zhao & Running, 2010) to assess the uncertainty of carbon input and its consequences on model-inferred structures of τ and a. Finally, we repeated the analyses using other three carbon model variates to test whether the results depend on model structure used to infer the PDF of τ and a.

3. Results

3.1. Mean Soil Carbon Age and Transit Time of Carbon Inputs

Radiocarbon-inferred $\overline{a}$ increases with soil depth (Figure 2a). Integrating $\overline{a}$ into the 0–30 and 30–100 cm soil layers, an average $\overline{a}$ of 1,707 and 3,161 years is estimated, respectively (Figure 2b). These estimates are in general smaller than the global estimates of $\overline{a}$ (1,390 and 8,280 years in the two depths, respectively) by Shi et al. (2020). This underestimation is reasonable as estimates of Shi et al. (2020) were based on global mapping products of radiocarbon, including tundra and permafrost regions (where soil carbon is much older than in other regions), which contributed more to their average than the 910 observed soil profiles (Figure 1). In the 100–200 cm soil layer, $\overline{a}$ is increased to 7,118 years (Figure 2b). Mean transit time ($\overline{\tau}$) also is increased with soil depth (Figure 2a), with an average $\overline{\tau}$ of 315, 489, and 931 years estimated in the three depths, respectively (Figure 2b).

10.1029/2023EF003982

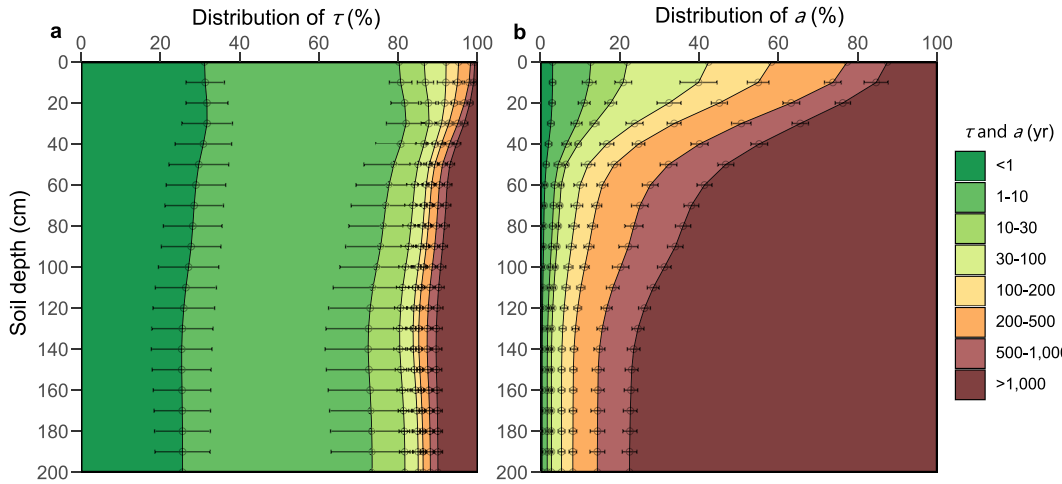

Figure 3. Depth distributions of transit time of carbon input (τ) and soil carbon age (a). A two-pool soil carbon model was used to estimate the distributions of τ and a in each 10 cm depth interval (Methods). Circles and error bars show the average and one standard deviation of the estimation, respectively.

3.2. Transit Behavior of Carbon Inputs

Most new carbon inputs transit fast and leave soil rapidly regardless of entering soil depth (Figure 3a). In all depths, on average ~25% of carbon inputs leave soil within the first year after entering, and another ~45% leave within the next 9 years (Figure 3b). Specifically, in the 0–30, 30–100, and 100–200 cm soil layers, on average 30.2% ± 4.7%, 28.9% ± 6.0% and 24.7% ± 7.6% of carbon inputs leave soil in 1 year, respectively. After 30 years, the remaining fraction is further reduced to 13.0% ± 4.6%, 15.3% ± 8.6% and 17.5% ± 9.9% in the three soil layers, respectively. At a significantly longer time scale, however, the transit of remaining carbon inputs does present an apparent vertical gradient (Figure 3a). After 1,000 years, for example, only 1.5% ± 1.4%, 6.4% ± 5.0% and 9.2% ± 5.9% of carbon inputs are remained in the three layers, respectively (Figure 3a).

Among biomes, the transit behavior of carbon inputs is significantly different (Figures 4a and 4b). In all soil depths, carbon inputs in colder biomes such as tundra, boreal forests and temperate forests transit slower, and less

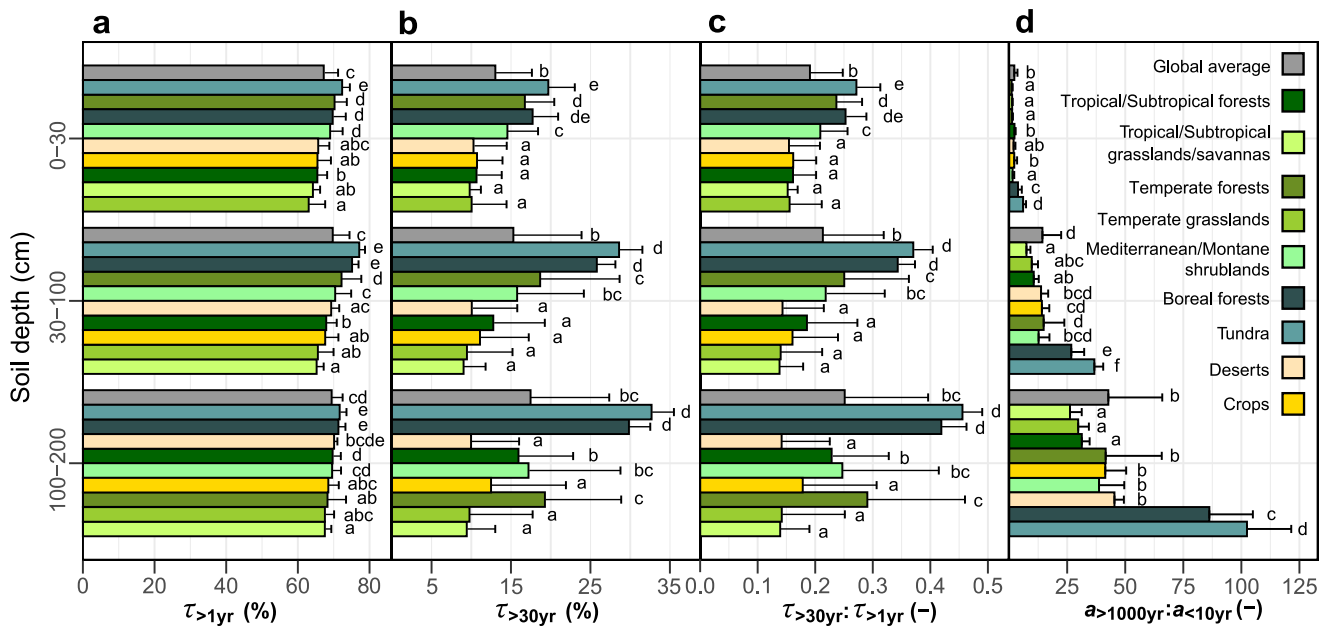

Figure 4. The proportion of selected groups of carbon input transit times (τ) and soil carbon age across depths and biomes. Error bars show one standard deviation. Within each group of a and τ or soil layer, and biomes followed by the same letter do not differ significantly ($p < 0.05$).

than 30% of carbon inputs leave soil in the first year after entering soil (Figure 4a). In other biomes, carbon inputs transit faster, and in general more than 30% of carbon inputs leave soil in the first year (Figure 4a). After 30 years of entering, the discrepancy of remaining fractions is substantially increased among the biomes (Figure 4b). The percentage of carbon inputs retained in boreal forests and tundra is nearly two times of that in other biomes, especially in the two deeper layers (Figure 4b). For example, in boreal forests, ∼18%, ∼26%, and ∼30% of carbon inputs are retained after 30 years of entering in the 0–30, 30–100, and 100–200 cm soil layers, respectively (Figure 4b). In temperate grasslands, however, only ∼10% of carbon inputs are retained after 30 years of entering in the three soil layers (Figure 4b). Long-period of low temperature in cold biomes such as boreal forests and tundra would inhibit the decomposition of carbon inputs and thus favoring long-term preservation of new carbon inputs.

By comparing the distributions of τ and a, we obtain some critical insights into the transfer efficiency of carbon inputs to aged carbon. It is apparent that SOC is mainly comprised of old carbon, especially in deeper depths (Figure 3b). Carbon being older than 30 years (which is a meaningful timescale for land management and SOC sequestration) account for more than three quarters (>75%) of SOC in all soil depths (Figure 3b). However, the fraction of carbon inputs transferred to this age group are minor (Figure 3a). In the 0–30, 30–100, and 100–200 cm layers, the average remaining fraction after 30 years is only 13.0% ± 4.6%, 15.3% ± 8.6%, and 17.5% ± 9.9%, respectively (Figure 4b).

3.3. Controls Over Carbon Input Transiting and SOC Aging

Given the distinct depth distributions of SOC ages and carbon input transit times, and that SOC is mainly comprised of aged carbon and most carbon inputs transit fast (Figures 3a vs. 3b), we propose that SOC aging and carbon input transiting may be two processes controlled by different environmental factors. To indicate carbon input transiting, we calculate the ratio of remaining carbon inputs after 30 years of entering to that after 1 year of entering ($\tau_{>30\ \text{years}}$:$\tau_{>1\ \text{year}}$, Figure 4c). This ratio in general is comparable among soil depths (Figure 4c). In the 0–30, 30–100, and 100–200 cm soil layers, the global average $\tau_{>30\ \text{years}}$:$\tau_{>1\ \text{year}}$ is 0.19 ± 0.06, 0.21 ± 0.11, and 0.25 ± 0.15, respectively. Among biomes, $\tau_{>30\ \text{years}}$:$\tau_{>1\ \text{year}}$ is relatively higher in tundra and boreal than those in other biomes in all three soil layers (Figure 4c).

The ratio of $a_{>1{,}000\ \text{years}}$ (the fraction of SOC being older than 1,000 years) to $a_{<10\ \text{years}}$ (the fraction of SOC being younger than 10 years), that is, $a_{>1{,}000\ \text{years}}$:$a_{<10\ \text{years}}$, is calculated to indicate SOC aging. A higher $a_{>1{,}000\ \text{years}}$:$a_{<10\ \text{years}}$ ratio indicates old carbon is more dominant in total SOC, and vice versa. Unlike $\tau_{>30\ \text{years}}$:$\tau_{>1\ \text{year}}$, the global average $a_{>1{,}000\ \text{years}}$:$a_{<10\ \text{years}}$ ratio is substantially increased with soil depth, and is estimated to be 2.2 ± 1.4, 14.3 ± 8.1, and 42.7 ± 23.2 in the three depths, respectively (Figure 4d). Among biomes, this ratio shows much greater variability in deeper layers. In the 100–200 cm soil layer depth, tropical/subtropical grasslands and savannas have the lowest $a_{>1{,}000\ \text{years}}$:$a_{<10\ \text{years}}$ ratio of 26.2 ± 5.1, followed by temperate grasslands (39.7 ± 4.6), while this ratio is increased to 102.4 ± 19.1 and 86.2 ± 18.7 in tundra and boreal forests, respectively (Figure 4d).

A VPA is conducted to assess drivers of $\tau_{>30\ \text{years}}$:$\tau_{>1\ \text{year}}$ and $a_{>1{,}000\ \text{years}}$:$a_{<10\ \text{years}}$ (Figure 5). The VPA driven by climatic, edaphic and topographic attributes (Methods) can explain 61%–77% variance of the two ratios in the three soil depths. For $\tau_{>30\ \text{years}}$:$\tau_{>1\ \text{year}}$, climate is more important (explaining 18%–22% of the variance alone) than soil (7%–15%) and topography (which has marginal effects of 1%–2%) in the three layers (Figures 5a, 5c, and 5e). However, the interactions between climate and soil plays the dominant role in the upper two layers (Figures 5a and 5c). In the 100–200 cm layer, the interaction between climate and soil shows the similar importance as climate alone (Figure 5e). For $a_{>1{,}000\ \text{years}}$:$a_{<10\ \text{years}}$, climate becomes more important and is the predominant control, particularly in deeper layers (Figures 5b, 5d, and 5f). Across all soil layers, climate alone explains 22%–42% of the variance of $a_{>1{,}000\ \text{years}}$:$a_{<10\ \text{years}}$, and its interaction with soil (i.e., edaphic properties) contributes additional 14%–29%, while soil alone and topographic properties have a marginal effect of 2%–10% (Figures 5b, 5d, and 5f).

3.4. Uncertainty Assessment of the Estimates

We tested the effects of some assumptions on our estimations. First, we have investigated potential uncertainties related to the accuracy of carbon input data set which are critical for estimating $\bar{\tau}$. Although the data set is derived from field measurements with machine learning models and has considered the depth distribution of root growth

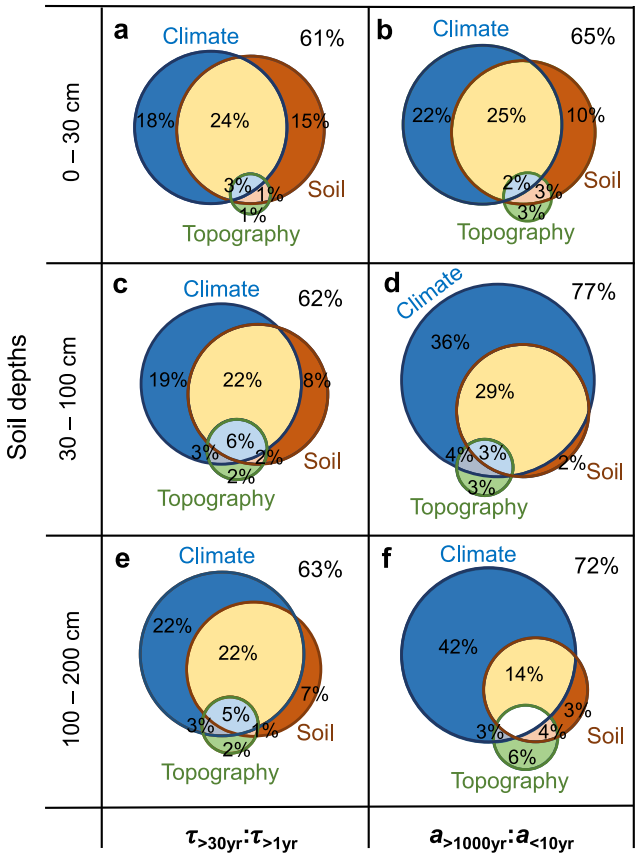

Figure 5. Variation partitioning modeling on transit time structure of carbon inputs ($\tau_{>30\ years}$:$\tau_{>1\ year}$) and age structure of soil carbon ($a_{>1,000\ years}$:$a_{<10\ years}$). Detailed climatic, edaphic and topographic variables were described in Table S1 in Supporting Information S1. Values in blank area show total variances explained by the variation partition analysis. Inset white area in sub-figure (f) shows 0%.

and turnover as well as the vertical transport of carbon inputs through soil profile, accurate measurement of depth-specific carbon inputs is still a grand challenge. We used the MODIS NPP product to derive carbon inputs for the 910 $\Delta^{14}C$ profiles. The result shows that both the magnitude of carbon inputs (Figures S1a and S1b in Supporting Information S1) and the associated estimations of the structure of τ and a (Figures S1c and S1d in Supporting Information S1) are comparable between the two data sets. Second, to infer $\overline{a}$ from a single $\Delta^{14}C$ measurement, a homogeneous, one-pool radiocarbon model was used. However, as soil carbon composition is heterogeneous, modeling a single pool would be too simplistic. The sensitivity analysis shows that ±10% changes of $\overline{a}$ do not significantly change the structures of a and τ (Figures S2a and S2b in Supporting Information S1). Again, ±10% changes of mean transit times have negligible effects on the results (Figures S2c and S2d in Supporting Information S1). Last, the calculation of age structure and transit times relies on the specific ICBM model. We tested their sensitivity to model structure by repeating all calculations using other three model varieties considering different carbon input partitioning and pool exchanges (Figure S3 in Supporting Information S1), and do not find significant effects of model structure on the overall patterns of the results (Figure S4 in Supporting Information S1). This tolerance of the estimation to different uncertainty sources would be due to that mean SOC age is much larger than mean carbon input transit time (Figure 2). As such, any subtle changes induced by the relevant uncertainties will have minor effects on the estimated distribution of SOC ages and carbon input transit times.

4. Discussion

The results reveal fast transit of carbon inputs in the whole soil profile regardless of entering depth. Our previous study focusing on mean transit times and ages (i.e., $\overline{a}$ and $\overline{\tau}$) has proposed a mechanism underpinning such fast transit (Wang et al., 2023; Xiao et al., 2022). That is, the majority of carbon inputs such as root litter and exudates may be quickly utilized and respired as CO_2 by microbes in the rhizosphere (Finzi et al., 2015; Fontaine et al., 2007; Zahar Haichar et al., 2014). Another possibility is that microbial decomposition of soil carbon is inherently limited by energy availability (Fontaine et al., 2007; Henneron et al., 2022; Lehmann & Kleber, 2015; Soong et al., 2020). Fresh carbon inputs are not only usually energy-rich (e.g., sugars and proteins) but also less involved in soil organo-mineral interactions that reduce the accessibility of carbon substrates to microbes. As such, new carbon inputs would be preferentially or easily used by soil microbes (Osler & Sommerkorn, 2007; Van Den Hoogen et al., 2019). The finding can help explain the neutral responses of SOC to carbon input changes observed in manipulative field experiments at the time scale of years up to several decades (Jiang et al., 2020; Kuzyakov et al., 2019; Terrer et al., 2019).

In deep soil, microbial decomposition may suffer from more depth-induced environmental constraints such as lower O_2 availability (Hartmann et al., 2014) and stronger organo-mineral interactions (Poirier et al., 2020). It is reasonable to expect slower decomposition of carbon inputs in deeper layers. However, such expectation is not supported by the depth-independent transit (Figure 3a). According to Liebig's law of the minimum, it is likely that those environmental constrains are still secondary compared to energy limitation in deeper soil layers (Henneron et al., 2022; Jones et al., 2018; Soong et al., 2020). Indeed, the carbon to nitrogen ratio (a lower value of which indicates lower energy content) usually decreases with soil depth (Jobbagy & Jackson, 2001). Carbon inputs in deep soil are mainly comprised of root debris and exudates, which usually have a higher C:N ratio and would be preferentially utilized by microbes to acquire energy. At later decomposition stages at the time scale of decades or centuries, remaining carbon inputs may have been microbially-processed and -recycled many times. These recycled carbon (e.g., microbial debris or necromass) are not energy-rich anymore, and their transit may be strongly mediated by physiochemical protection processes. This would be the reason of why aged soil carbon is dominant, particularly in deeper layers (Figure 3b).

Unlike earlier studies that focused on mean transit times and soil carbon age (i.e., $\overline{a}$ and $\overline{\tau}$), in this study, we quantitatively demonstrate that natural soil carbon capture is a slow process by estimating the fraction of carbon inputs transformed into different age groups of soil carbon. For instance, in the topsoil (0–30 cm), where the majority of carbon inputs are received (Wang et al., 2023), we show that only 2% of this input remains for over 1,000 years. This challenges the efficacy of managing carbon inputs (e.g., through land management or increased plant productivity) to enhance long-term soil carbon sequestration. Instead, it may be more practical to identify methods that can stabilize new carbon inputs (e.g., biochar application (Weng et al., 2017)), or identify locations where climate and soil conditions can preserve most new carbon inputs for extended periods, such as boreal forests, tundra, or deeper soil layers (Wang et al., 2023). Under global change and land use/management shifts, plant communities and their root systems and rooting depth may be altered (Lange et al., 2015; Sokol & Bradford, 2019) therefore redistributing carbon inputs through the soil profile. This may have significant long-term consequences on the vertical distribution of SOC storage along the soil profile. Promoting carbon input to deeper depths may be more effective for long-term SOC accumulation, but these effects may take a considerable time to become noticeable. In the modeling community, the predominant focus is on soil carbon dynamics in the upper layers (e.g., 0–30 cm), with limited attention given to the transiting of carbon inputs and soil carbon sequestration in deeper layers. Furthermore, the majority of existing models primarily address soil carbon transit behaviors, while only a few consider soil carbon aging processes, and even fewer integrate both aspects due to data availability and technological constraints. In this context, we propose that accounts for these two distinct processes regarding soil carbon input transit and soil carbon aging are vital. Most importantly, our estimates provide insights into improving the assessment and representation of diverse carbon transit behaviors across various soil depths within Earth system models, thereby facilitating more precise predictions of soil carbon dynamics across the entire soil profile in response to climate change and land management.

Climate and soil properties show depth-dependent, interactive and distinct effects on SOC aging and carbon input transiting (Figure 5). This phenomenon may be attributed to different mechanisms/controls that would act with the proceeding of the decomposition of carbon inputs (Lehmann & Kleber, 2015). Climate has an overall larger impact on SOC aging than carbon input transiting. A possible explanation is that climate influences both carbon input and output which form age structure, while soil properties influence more on the output/decomposition rate and soil aggregates formation that dominate the impacts on the transit time. Our previous study has demonstrated that climate is the most important regulator of mean SOC age (Wang et al., 2023; Xiao et al., 2022). For transit times, soil properties have been found to override climatic attributes controlling mean transit times of carbon inputs in the 30–100 cm soil depths (Luo et al., 2019). Another study focusing on soil carbon stock has also demonstrated that climatic and soil properties show similar importance for controlling the global spatial pattern of SOC stock (Luo et al., 2021). It is well recognized that SOC is comprised of a continuum of carbon compounds with different ages, and different carbon fractions (e.g., particulate and mineral-associated organic carbon) exert distinct response to climate and land use changes (Lugato et al., 2021; Luo et al., 2020). These results suggest that final SOC storage would be the combined and integrated consequences of the distinct decomposition and stabilization of those compounds with different ages at different transit stages.

5. Conclusion

Our study quantified the age structure of SOC and the transit behavior of plant-derived carbon inputs across different soil depths. We found that aged carbon (>30 years) dominates SOC in deeper layers, but most carbon inputs transit fast regardless of the depth of entering. In the topsoil (0–30 cm), where most carbon inputs occur, only a small fraction of them (~13%) stay longer than 30 years and contribute to long-term SOC sequestration. Our estimations can help improve testing and represent distinct carbon transit behaviors with the proceeding of decomposition across depths in Earth system models, thereby promoting reliable prediction of whole-profile SOC dynamics in response to climate change and land management.

Data Availability Statement

The data that support the findings of this study can be downloaded from figshare (Wang, 2022).

Acknowledgments
This research has been financially supported by the National Key Research Program of the Ministry of Science and Technology of China (Grant 2021YFE0114500), the National Natural Science Foundation of China (Grants 32241036, 32171639, and 42375116) and the Fundamental Research Funds for the Central Universities.

References

Amatulli, G., Domisch, S., Tuanmu, M.-N., Parmentier, B., Ranipeta, A., Malczyk, J., & Jetz, W. (2018). A suite of global, cross-scale topographic variables for environmental and biodiversity modeling. *Scientific Data*, *5*(1), 1–15. https://doi.org/10.1038/sdata.2018.40

Andrén, O., & Kätterer, T. (1997). ICBM: The introductory carbon balance model for exploration of soil carbon balances. *Ecological Applications*, *7*(4), 1226–1236. https://doi.org/10.1890/1051-0761(1997)007[1226:ITICBM]2.0.CO;2

Balesdent, J., Basile-Doelsch, I., Chadoeuf, J., Cornu, S., Derrien, D., Fekiacova, Z., & Hatté, C. (2018). Atmosphere–soil carbon transfer as a function of soil depth. *Nature*, *559*(7715), 599–602. https://doi.org/10.1038/s41586-018-0328-3

Batjes, N. H. (2016). Harmonized soil property values for broad-scale modelling (WISE30sec) with estimates of global soil carbon stocks. *Geoderma*, *269*, 61–68. https://doi.org/10.1016/j.geoderma.2016.01.034

Bishop, T. F. A., McBratney, A. B., & Laslett, G. M. (1999). Modelling soil attribute depth functions with equal-area quadratic smoothing splines. *Geoderma*, *91*(1), 27–45. https://doi.org/10.1016/S0016-7061(99)00003-8

Carvalhais, N., Forkel, M., Khomik, M., Bellarby, J., Jung, M., Migliavacca, M., et al. (2014). Global covariation of carbon turnover times with climate in terrestrial ecosystems. *Nature*, *514*(7521), 213–217. https://doi.org/10.1038/nature13731

Cherkinsky, A., & Brovkin, V. (1993). Dynamics of radiocarbon in soils. *Radiocarbon*, *35*(3), 363–367. https://doi.org/10.1017/s0033822200060367

Crowther, T. W., Todd-Brown, K. E., Rowe, C. W., Wieder, W. R., Carey, J. C., Machmuller, M. B., et al. (2016). Quantifying global soil carbon losses in response to warming. *Nature*, *540*(7631), 104–108. https://doi.org/10.1038/nature20150

Fick, S. E., & Hijmans, R. J. (2017). WorldClim 2: New 1-km spatial resolution climate surfaces for global land areas. *International Journal of Climatology*, *37*(12), 4302–4315. https://doi.org/10.1002/joc.5086

Finzi, A. C., Abramoff, R. Z., Spiller, K. S., Brzostek, E. R., Darby, B. A., Kramer, M. A., & Phillips, R. P. (2015). Rhizosphere processes are quantitatively important components of terrestrial carbon and nutrient cycles. *Global Change Biology*, *21*(5), 2082–2094. https://doi.org/10.1111/gcb.12816

Fontaine, S., Barot, S., Barré, P., Bdioui, N., Mary, B., & Rumpel, C. (2007). Stability of organic carbon in deep soil layers controlled by fresh carbon supply. *Nature*, *450*(7167), 277–280. https://doi.org/10.1038/nature06275

Hartmann, M., Niklaus, P. A., Zimmermann, S., Schmutz, S., Kremer, J., Abarenkov, K., et al. (2014). Resistance and resilience of the forest soil microbiome to logging-associated compaction. *ISME Journal*, *8*(1), 226–244. https://doi.org/10.1038/ismej.2013.141

Henneron, L., Balesdent, J., Alvarez, G., Barré, P., Baudin, F., Basile-Doelsch, I., et al. (2022). Bioenergetic control of soil carbon dynamics across depth. *Nature Communications*, *13*(1), 7676. https://doi.org/10.1038/s41467-022-34951-w

Hogg, A. G., Heaton, T. J., Hua, Q., Palmer, J. G., Turney, C. S. M., Southon, J., et al. (2020). SHCal20 Southern Hemisphere calibration, 0–55,000 years cal BP. *Radiocarbon*, *62*(4), 759–778. https://doi.org/10.1017/RDC.2020.59

Hua, Q., Turnbull, J. C., Santos, G. M., Rakowski, A. Z., Ancapichún, S., De Pol-Holz, R., et al. (2021). Atmospheric radiocarbon for the period 1950–2019. In *Radiocarbon* (pp. 1–23). Retrieved from https://www.cambridge.org/core/article/atmospheric-radiocarbon-for-the-period-19502019/28F8E4DD4BA3F32266541445EC3F64C8

Jackson, R. B., Lajtha, K., Crow, S. E., Hugelius, G., Kramer, M. G., & Piñeiro, G. (2017). The ecology of soil carbon: Pools, vulnerabilities, and biotic and abiotic controls. *Annual Review of Ecology, Evolution, and Systematics*, *48*(1), 419–445. https://doi.org/10.1146/annurev-ecolsys-112414-054234

Jiang, M., Medlyn, B. E., Drake, J. E., Duursma, R. A., Anderson, I. C., Barton, C. V. M., et al. (2020). The fate of carbon in a mature forest under carbon dioxide enrichment. *Nature*, *580*(7802), 227–231. https://doi.org/10.1038/s41586-020-2128-9

Jobbágy, E. G., & Jackson, R. B. (2000). The vertical distribution of soil organic carbon and its relation to climate and vegetation. *Ecological Applications*, *10*(2), 423–436. https://doi.org/10.1890/1051-0761(2000)010[0423:Tvdoso]2.0.Co;2

Jobbagy, E. G., & Jackson, R. B. (2001). The distribution of soil nutrients with depth: Global patterns and the imprint of plants. *Biogeochemistry*, *53*(1), 51–77. https://doi.org/10.1023/a:1010760720215

Jones, D. L., Magthab, E. A., Gleeson, D. B., Hill, P. W., Sánchez-Rodríguez, A. R., Roberts, P., et al. (2018). Microbial competition for nitrogen and carbon is as intense in the subsoil as in the topsoil. *Soil Biology and Biochemistry*, *117*, 72–82. https://doi.org/10.1016/j.soilbio.2017.10.024

Koven, C., Riley, W., Subin, Z., Tang, J., Torn, M., Collins, W., et al. (2013). The effect of vertically resolved soil biogeochemistry and alternate soil C and N models on C dynamics of CLM4. *Biogeosciences*, *10*(11), 7109–7131. https://doi.org/10.5194/bg-10-7109-2013

Kuzyakov, Y., Horwath, W. R., Dorodnikov, M., & Blagodatskaya, E. (2019). Review and synthesis of the effects of elevated atmospheric CO_2 on soil processes: No changes in pools, but increased fluxes and accelerated cycles. *Soil Biology and Biochemistry*, *128*, 66–78. https://doi.org/10.1016/j.soilbio.2018.10.005

Lal, R. (2004). Soil carbon sequestration impacts on global climate change and food security. *Science*, *304*(5677), 1623–1627. https://doi.org/10.1126/science.1097396

Lange, M., Eisenhauer, N., Sierra, C. A., Bessler, H., Engels, C., Griffiths, R. I., et al. (2015). Plant diversity increases soil microbial activity and soil carbon storage. *Nature Communications*, *6*(1), 6707. https://doi.org/10.1038/ncomms7707

Lawrence, C. R., Beem-Miller, J., Hoyt, A. M., Monroe, G., Sierra, C. A., Stoner, S., et al. (2020). An open-source database for the synthesis of soil radiocarbon data: International Soil Radiocarbon Database (ISRaD) version 1.0. *Earth System Science Data*, *12*(1), 61–76. https://doi.org/10.5194/essd-12-61-2020

Lehmann, J., & Kleber, M. (2015). The contentious nature of soil organic matter. *Nature*, *528*(7580), 60–68. https://doi.org/10.1038/nature16069

Lugato, E., Lavallee, J. M., Haddix, M. L., Panagos, P., & Cotrufo, M. F. (2021). Different climate sensitivity of particulate and mineral-associated soil organic matter. *Nature Geoscience*, *14*(5), 295–300. https://doi.org/10.1038/s41561-021-00744-x

Luo, Z., Viscarra-Rossel, R. A., & Qian, T. (2021). Similar importance of edaphic and climatic factors for controlling soil organic carbon stocks of the world. *Biogeosciences*, *18*(6), 2063–2073. https://doi.org/10.5194/bg-18-2063-2021

Luo, Z., Viscarra Rossel, R. A., & Shi, Z. (2020). Distinct controls over the temporal dynamics of soil carbon fractions after land use change. *Global Change Biology*, *26*(8), 4614–4625. https://doi.org/10.1111/gcb.15157

Luo, Z., Wang, G., & Wang, E. (2019). Global subsoil organic carbon turnover times dominantly controlled by soil properties rather than climate. *Nature Communications*, *10*(1), 3688. https://doi.org/10.1038/s41467-019-11597-9

Metzler, H., & Sierra, C. A. (2018). Linear autonomous compartmental models as continuous-time Markov chains: Transit-time and age distributions. *Mathematical Geosciences*, *50*(1), 1–34. https://doi.org/10.1007/s11004-017-9690-1

Osler, G. H., & Sommerkorn, M. (2007). Toward a complete soil C and N cycle: Incorporating the soil fauna. *Ecology*, *88*(7), 1611–1621. https://doi.org/10.1890/06-1357.1

Peres-Neto, P. R., Legendre, P., Dray, S., & Borcard, D. (2006). Variation partitioning of species data matrices: Estimation and comparison of fractions. *Ecology*, *87*(10), 2614–2625. https://doi.org/10.1890/0012-9658(2006)87[2614:vposdm]2.0.co;2

Poirier, V., Basile-Doelsch, I., Balesdent, J., Borschneck, D., Whalen, J. K., & Angers, D. A. (2020). Organo-mineral interactions are more important for organic matter retention in subsoil than topsoil. *Soil Systems*, *4*(1), 4. https://doi.org/10.3390/soilsystems4010004

R Development Core Team. (2023). R: A language and environment for statistical computing. In *R foundation for statistical computing*. Retrieved from http://www.R-project.org

Reimer, P. J., Austin, W. E. N., Bard, E., Bayliss, A., Blackwell, P. G., Bronk Ramsey, C., et al. (2020). The IntCal20 Northern Hemisphere radiocarbon age calibration curve (0–55 cal kBP). *Radiocarbon*, *62*(4), 725–757. https://doi.org/10.1017/RDC.2020.41

Shi, Z., Allison, S. D., He, Y., Levine, P. A., Hoyt, A. M., Beem-Miller, J., et al. (2020). The age distribution of global soil carbon inferred from radiocarbon measurements. *Nature Geoscience*, *13*(8), 555–559. https://doi.org/10.1038/s41561-020-0596-z

Sierra, C. A., Hoyt, A. M., He, Y., & Trumbore, S. E. (2018). Soil organic matter persistence as a stochastic process: Age and transit time distributions of carbon in soils. *Global Biogeochemical Cycles*, *32*(10), 1574–1588. https://doi.org/10.1029/2018GB005950

Sierra, C. A., Müller, M., Metzler, H., Manzoni, S., & Trumbore, S. E. (2017). The muddle of ages, turnover, transit, and residence times in the carbon cycle. *Global Change Biology*, *23*(5), 1763–1773. https://doi.org/10.1111/gcb.13556

Sokol, N. W., & Bradford, M. A. (2019). Microbial formation of stable soil carbon is more efficient from belowground than aboveground input. *Nature Geoscience*, *12*(1), 46–53. https://doi.org/10.1038/s41561-018-0258-6

Song, J., Wan, S., Piao, S., Knapp, A. K., Classen, A. T., Vicca, S., et al. (2019). A meta-analysis of 1,119 manipulative experiments on terrestrial carbon-cycling responses to global change. *Nature Ecology & Evolution*, *3*(9), 1309–1320. https://doi.org/10.1038/s41559-019-0958-3

Soong, J. L., Fuchslueger, L., Marañon-Jimenez, S., Torn, M. S., Janssens, I. A., Penuelas, J., & Richter, A. (2020). Microbial carbon limitation: The need for integrating microorganisms into our understanding of ecosystem carbon cycling. *Global Change Biology*, *26*(4), 1953–1961. https://doi.org/10.1111/gcb.14962

Terrer, C., Jackson, R. B., Prentice, I. C., Keenan, T. F., Kaiser, C., Vicca, S., et al. (2019). Nitrogen and phosphorus constrain the CO_2 fertilization of global plant biomass. *Nature Climate Change*, *9*(9), 684–689. https://doi.org/10.1038/s41558-019-0545-2

Terrer, C., Phillips, R. P., Hungate, B. A., Rosende, J., Pett-Ridge, J., Craig, M. E., et al. (2021). A trade-off between plant and soil carbon storage under elevated CO_2. *Nature*, *591*(7851), 599–603. https://doi.org/10.1038/s41586-021-03306-8

Van Den Hoogen, J., Geisen, S., Routh, D., Ferris, H., Traunspurger, W., Wardle, D. A., et al. (2019). Soil nematode abundance and functional group composition at a global scale. *Nature*, *572*(7768), 194–198. https://doi.org/10.1038/s41586-019-1418-6

Vrugt, J. A., & Ter Braak, C. J. F. (2011). $DREAM_{(D)}$: An adaptive Markov Chain Monte Carlo simulation algorithm to solve discrete, noncontinuous, and combinatorial posterior parameter estimation problems. *Hydrology and Earth System Sciences*, *15*(12), 3701–3713. https://doi.org/10.5194/hess-15-3701-2011

Wang, G. (2022). Distribution of soil carbon age and carbon input transit times (Version 2) [Dataset]. figshare. https://doi.org/10.6084/m9.figshare.20409360.v2

Wang, G., Xiao, L., Lin, Z., Zhang, Q., Guo, X., Cowie, A., et al. (2023). Most root-derived carbon inputs do not contribute to long-term global soil carbon storage. *Science China Earth Sciences*, *66*(5), 1072–1086. https://doi.org/10.1007/s11430-022-1031-5

Weng, Z., Van Zwieten, L., Singh, B. P., Tavakkoli, E., Joseph, S., Macdonald, L. M., et al. (2017). Biochar built soil carbon over a decade by stabilizing rhizodeposits. *Nature Climate Change*, *7*(5), 371–376. https://doi.org/10.1038/nclimate3276

Xiao, L., Wang, G., Chang, J., Chen, Y., Guo, X., Mao, X., et al. (2023). Global depth distribution of belowground net primary productivity and its drivers. *Global Ecology and Biogeography*, *32*(8), 1435–1451. https://doi.org/10.1111/geb.13705

Xiao, L., Wang, G., Wang, M., Zhang, S., Sierra, C. A., Guo, X., et al. (2022). Younger carbon dominates global soil carbon efflux. *Global Change Biology*, *28*(18), 5587–5599. Retrieved from https://onlinelibrary.wiley.com/doi/abs/10.1111/gcb.16311

Zahar Haichar, F., Santaella, C., Heulin, T., & Achouak, W. (2014). Root exudates mediated interactions belowground. *Soil Biology and Biochemistry*, *77*, 69–80. https://doi.org/10.1016/j.soilbio.2014.06.017

Zhao, M., & Running, S. W. (2010). Drought-induced reduction in global terrestrial net primary production from 2000 through 2009. *Science*, *329*(5994), 940–943. https://doi.org/10.1126/science.1192666

Zuur, A. F., Ieno, E. N., & Elphick, C. S. (2010). A protocol for data exploration to avoid common statistical problems. *Methods in Ecology and Evolution*, *1*(1), 3–14. https://doi.org/10.1111/j.2041-210x.2009.00001.x